Reduced order models for railway induced vibration based on the proper generalized decomposition

G. Herremans, S. François, G. Degrande
KU Leuven, Department of Civil Engineering,
Kasteelpark Arenberg 40 box 2448, B-3001, Leuven, Belgium

Abstract
A model order reduction technique, the Proper Generalized Decomposition (PGD), is presented for the assessment of railway induced vibration. The methodology is elaborated for 2.5D track-soil models exploiting the geometrical invariance of the track and soil. Firstly, the standard PGD methodology is described. The formulation is introduced for a beam on a Winkler foundation and extended to a 2.5D ballast track. Secondly, two alternative PGD formulations are discussed: a Petrov-Galerkin and a minimal residual approach. Results are compared for the beam on a Winkler foundation and the 2.5D ballast track. The latter is discussed for both a homogeneous and layered halfspace. The Petrov-Galerkin converges slightly faster. A possible explanation is that the system is non-Hermitian. The minimal residual approach performs poorly for the 2.5D ballast track in terms of CPU time and convergence.

1 Introduction

An increase in urban and high speed railway lines has been noted worldwide, as railways are more environmentally friendly in terms of energy consumption, CO_2 and exhaust atmospheric emission. Multiple challenges arise in the field of railway engineering as the source problem is a complex dynamic soil-structure interaction problem that has to be evaluated for a wide frequency range (up to 80 Hz). The large number of determining parameters asks for large-scale parametric studies.

Three-dimensional (3D) numerical models have been developed to assess the track as well as soil response, based on the finite element method (FEM), boundary element method (BEM) [1] and the FEM combined with Perfectly Matched Layers (PMLs) [2]. In an effort to reduce numerical complexity, two-and-a-half dimensional (2.5D) models [3, 4] were developed, assuming the track and soil to be longitudinally invariant. Although this reduces computational efforts, extensive studies are still hindered due to the curse of dimensionality.

This paper proposes a reduced order strategy to assess vibration in 2.5D track models. The Proper Generalised Decomposition (PGD) [5, 6, 7] provides a computational vademecum, computed in an offline phase, in a low-rank format. The full solution can subsequently be generated in the online phase, when the parameter combination is specified. In contrast to classical a posteriori reduced order methods, PGD computes a reduced order solution a priori and no new solves are required in the online stage. The PGD terms are added in a greedy manner and consist of products of low dimensional functions, resulting in a separated representation of the solution [8]. The technique has already been successfully applied to dynamic problems [8, 9, 10, 11], although studies are often focused on results in the low-frequency band.

This paper aims to extend the PGD formulation to higher frequency bands as well as to study the use of PGD in a multi-parameter context for 2.5D track models coupled with BEM. The PGD formulation is first elaborated for a simplified model consisting of a beam on a Winkler foundation. The stiffness of the foundation is added as an additional parameter to illustrate the use of PGD for parametric problems. Next, the methodology is extended to the case of a 2.5D ballast track, where the spatial variation and frequency are incorporated as variables. Results are presented for a beam on a Winkler foundation and a 2.5D ballast track

supported by both a homogeneous halfspace and a layer on a halfspace, comparing the performance of all algorithms in terms of both convergence and CPU time.

2 Proper Generalized Decomposition

The Proper Generalized Decomposition (PGD) provides a strategy for solving high-dimensional problems by introducing a separable representation of the solution as a sum of rank-one tensors:

$$\mathbf{u}(\theta_1, \theta_2, \ldots, \theta_N) \approx \sum_{r_u=1}^{R_u} \bigotimes_{k=1}^{N} \mathbf{u}_k^{r_u}(\theta_k) \tag{1}$$

where the variables θ_k (with $k = 1 \ldots N$) denote all system variables, but can also represent additional problem parameters. All functions $\mathbf{u}_k^{r_u}(\theta_k)$ are unknown a priori. The solution is computed using successive enrichments, where each enrichment is added in a greedy manner. The optimal functions are computed using a Galerkin projection as illustrated in detail in section 2.1 for a beam on a Winkler foundation. The formulation is extended to a 2.5D ballast track in section 2.2

2.1 PGD for a beam on a Winkler foundation

The PGD strategy is elaborated for a beam on a Winkler foundation. This simplified geometry allows illustration of the methodology and can easily be generalized. The model consists of an Euler-Bernoulli beam, coupled with a Winkler foundation, accounting for the vertical spring stiffness and hysteretic damping. This support is assumed to be invariant with respect to the longitudinal coordinate, allowing the y coordinate to be transformed to the wavenumber k_y. The beam is loaded with a vertical load. The vertical equilibrium equation can be formulated in the wavenumber-frequency domain:

$$\left[-\rho_{\mathrm{r}} A_{\mathrm{r}} \omega^2 + (1 + \mathrm{i}\eta_{\mathrm{rp}})\bar{k}_{\mathrm{rp}} + E_{\mathrm{r}} I_{\mathrm{r}} k_y^4\right] \tilde{u}_z(k_y, \omega) = \tilde{f}_z(k_y, \omega) \tag{2}$$

where i is the imaginary unit, $\rho_{\mathrm{r}} A_{\mathrm{r}}$ is the beam's mass per unit length and $E_{\mathrm{r}} I_{\mathrm{r}}$ its bending stiffness. $\bar{k}_{\mathrm{rp}}$ is the foundation stiffness per unit length and η_{rp} the loss factor.

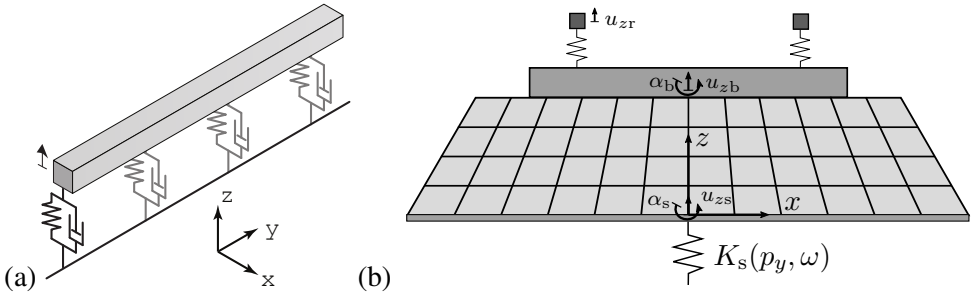

Figure 1: (a) Euler-Bernoulli beam on a Winkler foundation [12], and (b) 2.5D ballast track model consisting of rails, sleepers and ballast, coupled with a BE mesh for the underlying layered halfspace.

The equilibrium equation is solved for a range of wavenumbers in the domain I_{k_y} and frequencies in I_ω. The displacement $\tilde{u}_z(k_y, \omega, \bar{k}_{\mathrm{rp}})$ is therefore identified with a function defined on $I_{k_y} \otimes I_\omega$ with values in $\mathcal{K}_{k_y} \otimes \mathcal{K}_\omega$. The spring stiffness $\bar{k}_{\mathrm{rp}}$ is considered as an extra parameter with domain $I_{\bar{k}_{\mathrm{rp}}}$ and values in $\mathcal{K}_{\bar{k}_{\mathrm{rp}}}$. A weighted residual formulation is introduced:

Find $\tilde{u}_z \in \mathcal{K}_{k_y} \otimes \mathcal{K}_\omega \otimes \mathcal{K}_{\bar{k}_{\mathrm{rp}}}$ such that :

$$\int_{I_{k_y}\times I_\omega \times I_{\bar{k}_{\mathrm{rp}}}} \tilde{v}_z \cdot \left[-\rho_{\mathrm{r}} A_{\mathrm{r}} \omega^2 + (1+\mathrm{i}\eta_{\mathrm{rp}})\bar{k}_{\mathrm{rp}} + E_{\mathrm{r}} I_{\mathrm{r}} k_y^4\right] \tilde{u}_z \, \mathrm{d}k_y \mathrm{d}\omega \mathrm{d}\bar{k}_{\mathrm{rp}} = \int_{I_{k_y}\times I_\omega \times I_{\bar{k}_{\mathrm{rp}}}} \tilde{v}_z \cdot \tilde{f}_z \, \mathrm{d}k_y \mathrm{d}\omega \mathrm{d}\bar{k}_{\mathrm{rp}}$$
$$\forall \, \tilde{v}_z \in \mathcal{K}_{k_y} \otimes \mathcal{K}_\omega \otimes \mathcal{K}_{\bar{k}_{\mathrm{rp}}} \quad (3)$$

The weighted residual form is valid for any virtual displacement field $\tilde{v}_z(k_y, \omega, \bar{k}_{\mathrm{rp}})$ and states that the residual has to be orthogonal to the test functions. As a weighted residual formulation is introduced in all subdomains, integration is performed along all variables.

To solve this problem, an approximate solution is proposed of the form:

$$\tilde{u}_z\left(k_y, \omega, \bar{k}_{\mathrm{rp}}\right) \simeq \sum_{r_u=1}^{R_u+1} u_{k_y}^{r_u}(k_y) u_\omega^{r_u}(\omega) u_{\bar{k}_{\mathrm{rp}}}^{r_u}(\bar{k}_{\mathrm{rp}}) \quad (4)$$

where the wavenumber ($u_{k_y}^{r_u}(k_y) \in \mathcal{K}_{k_y}$), frequency ($u_\omega^{r_u}(\omega) \in \mathcal{K}_\omega$) and rail pad stiffness ($u_{\bar{k}_{\mathrm{rp}}}^{r_u}(\bar{k}_{\mathrm{rp}} \in \mathcal{K}_{\bar{k}_{\mathrm{rp}}}$) functions form low-dimensional reduced bases for their respective domains. The solution is therefore decomposed as a sum of R_u rank-1 contributions as proposed by the PGD formulation. As R_u enrichments have already been computed, the methodology aims to compute the (R_u+1)-th rank-1 contribution.

A discretization is introduced for all variables using a constant step size, resulting in N_{k_y}, N_ω and $N_{\bar{k}_{\mathrm{rp}}}$ samples for the wavenumber, frequency and rail pad stiffness domain, respectively. The discretized displacement field is given by:

$$\tilde{u}_z\left(k_y, \omega, \bar{k}_{\mathrm{rp}}\right) \simeq \sum_{r_u=1}^{R_u+1} \left(\mathbf{N}_{k_y}^{\mathrm{T}} \underline{\mathbf{u}}_{k_y}^{r_u}\right) \left(\mathbf{N}_\omega^{\mathrm{T}} \underline{\mathbf{u}}_\omega^{r_u}\right) \left(\mathbf{N}_{\bar{k}_{\mathrm{rp}}}^{\mathrm{T}} \underline{\mathbf{u}}_{\bar{k}_{\mathrm{rp}}}^{r_u}\right) \quad (5)$$

where the vector $\underline{\mathbf{u}}_k^{r_u}$ provides the nodal values for variable k, while the matrix $\mathbf{N}_k$ contains the shape functions in the respective domain. The same discretization is applied to the test functions, resulting in the following discretization:

$$\tilde{v}_z\left(k_y, \omega, \bar{k}_{\mathrm{rp}}\right) \simeq \left(\mathbf{N}_{k_y}^{\mathrm{T}} \underline{\mathbf{v}}_{k_y}\right) \left(\mathbf{N}_\omega^{\mathrm{T}} \underline{\mathbf{v}}_\omega\right) \left(\mathbf{N}_{\bar{k}_{\mathrm{rp}}}^{\mathrm{T}} \underline{\mathbf{v}}_{\bar{k}_{\mathrm{rp}}}\right) \quad (6)$$

Both formulations are introduced in the weighted residual equation:

Find $\underline{\mathbf{u}}_{k_y}^{R_u+1} \in \mathbb{C}^{N_{k_y}}, \underline{\mathbf{u}}_\omega^{R_u+1} \in \mathbb{C}^{N_\omega}$ and $\underline{\mathbf{u}}_{\bar{k}_{\mathrm{rp}}}^{R_u+1} \in \mathbb{C}^{N_{\bar{k}_{\mathrm{rp}}}}$ such that :

$$\int_{I_{k_y}\times I_\omega \times I_{\bar{k}_{\mathrm{rp}}}} \left[\left(\mathbf{N}_{k_y}^{\mathrm{T}} \underline{\mathbf{v}}_{k_y}\right) \otimes \left(\mathbf{N}_\omega^{\mathrm{T}} \underline{\mathbf{v}}_\omega\right) \otimes \left(\mathbf{N}_{\bar{k}_{\mathrm{rp}}}^{\mathrm{T}} \underline{\mathbf{v}}_{\bar{k}_{\mathrm{rp}}}\right)\right]^{\mathbf{H}}$$
$$\left[-\rho_{\mathrm{r}} A_{\mathrm{r}} \omega^2 + (1+\mathrm{i}\eta_{\mathrm{rp}})\bar{k}_{\mathrm{rp}} + E_{\mathrm{r}} I_{\mathrm{r}} k_y^4\right]$$
$$\sum_{r_u=1}^{R_u+1} \left[\left(\mathbf{N}_{k_y}^{\mathrm{T}} \underline{\mathbf{u}}_{k_y}^{r_u}\right) \otimes \left(\mathbf{N}_\omega^{\mathrm{T}} \underline{\mathbf{u}}_\omega^{r_u}\right) \otimes \left(\mathbf{N}_{\bar{k}_{\mathrm{rp}}}^{\mathrm{T}} \underline{\mathbf{u}}_{\bar{k}_{\mathrm{rp}}}^{r_u}\right)\right] \mathrm{d}k_y \mathrm{d}\omega \mathrm{d}\bar{k}_{\mathrm{rp}}$$
$$= \int_{I_{k_y}\times I_\omega \times I_{\bar{k}_{\mathrm{rp}}}} \left[\left(\mathbf{N}_{k_y}^{\mathrm{T}} \underline{\mathbf{v}}_{k_y}\right) \otimes \left(\mathbf{N}_\omega^{\mathrm{T}} \underline{\mathbf{v}}_\omega\right) \otimes \left(\mathbf{N}_{\bar{k}_{\mathrm{rp}}}^{\mathrm{T}} \underline{\mathbf{v}}_{\bar{k}_{\mathrm{rp}}}\right)\right]^{\mathbf{H}} \tilde{f}_z \, \mathrm{d}k_y \mathrm{d}\omega \mathrm{d}\bar{k}_{\mathrm{rp}}$$
$$\forall \, \underline{\mathbf{v}}_{k_y} \in \mathbb{C}^{N_{k_y}}, \, \underline{\mathbf{v}}_\omega \in \mathbb{C}^{N_\omega}, \, \underline{\mathbf{v}}_{\bar{k}_{\mathrm{rp}}} \in \mathbb{C}^{N_{\bar{k}_{\mathrm{rp}}}} \quad (7)$$

In order to allow efficient multiplication with the shape functions, the force vector $\tilde{f}_z$ has to be separable

with respect to the considered variables:

$$\tilde{f}_z = \sum_{r_f=1}^{R_f} \mathbf{f}_{k_y}^{r_f} \otimes \mathbf{f}_{\omega}^{r_f} \otimes \mathbf{f}_{\bar{k}_{\mathrm{rp}}}^{r_f} \tag{8}$$

Grouping all unknowns on the left hand side, the problem can be stated as:

$$\text{Find } \underline{\mathbf{u}}_{k_y}^{R_u+1} \in \mathbb{C}^{N_{k_y}}, \underline{\mathbf{u}}_{\omega}^{R_u+1} \in \mathbb{C}^{N_\omega} \text{ and } \underline{\mathbf{u}}_{\bar{k}_{\mathrm{rp}}}^{R_u+1} \in \mathbb{C}^{N_{\bar{k}_{\mathrm{rp}}}} \text{ such that :}$$
$$\mathcal{V}^{\mathbf{H}} \mathcal{A} \mathcal{U}_0 = \mathcal{V}^{\mathbf{H}} \mathcal{F} - \mathcal{V}^{\mathbf{H}} \mathcal{A} \mathcal{U} \qquad \forall\, \underline{\mathbf{v}}_{k_y} \in \mathbb{C}^{\mathrm{N}_{k_y}},\ \underline{\mathbf{v}}_{\omega} \in \mathbb{C}^{\mathrm{N}_\omega},\ \underline{\mathbf{v}}_{\bar{k}_{\mathrm{rp}}} \in \mathbb{C}^{\mathrm{N}_{\bar{k}_{\mathrm{rp}}}} \tag{9}$$

with $\mathcal{U}_0$ a tensor containing all nodal values computed in previous enrichments:

$$\mathcal{U}_0 = \sum_{r_u=1}^{R_u} \underline{\mathbf{u}}_{k_y}^{r_u} \otimes \underline{\mathbf{u}}_{\omega}^{r_u} \otimes \underline{\mathbf{u}}_{\bar{k}_{\mathrm{rp}}}^{r_u} \tag{10}$$

$\mathcal{U}$ a tensor containing all unknown nodal values:

$$\mathcal{U} = \underline{\mathbf{u}}_{k_y}^{R_u+1} \otimes \underline{\mathbf{u}}_{\omega}^{R_u+1} \otimes \underline{\mathbf{u}}_{\bar{k}_{\mathrm{rp}}}^{R_u+1} \tag{11}$$

$\mathcal{V}$ a tensor with the nodal values of the test functions:

$$\mathcal{V} = \underline{\mathbf{v}}_{k_y} \otimes \underline{\mathbf{v}}_{\omega} \otimes \underline{\mathbf{v}}_{\bar{k}_{\mathrm{rp}}} \tag{12}$$

$\mathcal{F}$ the force operator:

$$\mathcal{F} = \sum_{r_f=1}^{R_f} \int_{I_{k_y}} \mathbf{N}_{k_y} \mathbf{f}_{k_y}^{r_f} \mathrm{d}k_y \otimes \int_{I_\omega} \mathbf{N}_\omega \mathbf{f}_{\omega}^{r_f} \mathrm{d}\omega \otimes \int_{I_{\bar{k}_{\mathrm{rp}}}} \mathbf{N}_{\bar{k}_{\mathrm{rp}}} \mathbf{f}_{\bar{k}_{\mathrm{rp}}}^{r_f} \mathrm{d}\bar{k}_{\mathrm{rp}} \tag{13}$$

and $\mathcal{A}$ the stiffness operator:

$$\begin{aligned}\mathcal{A} = \rho_{\mathrm{r}} A_{\mathrm{r}} \int_{I_{k_y}} \mathbf{N}_{k_y} \mathbf{N}_{k_y}^T \mathrm{d}k_y \otimes \int_{I_\omega} -\omega^2 \mathbf{N}_\omega \mathbf{N}_\omega^T \mathrm{d}\omega \otimes \int_{I_{\bar{k}_{\mathrm{rp}}}} \mathbf{N}_{\bar{k}_{\mathrm{rp}}} \mathbf{N}_{\bar{k}_{\mathrm{rp}}}^T \mathrm{d}\bar{k}_{\mathrm{rp}} + \\ (1 + \mathrm{i}\eta_{\mathrm{rp}}) \int_{I_{k_y}} \mathbf{N}_{k_y} \mathbf{N}_{k_y}^T \mathrm{d}k_y \otimes \int_{I_\omega} \mathbf{N}_\omega \mathbf{N}_\omega^T \mathrm{d}\omega \otimes \int_{I_{\bar{k}_{\mathrm{rp}}}} \bar{k}_{\mathrm{rp}} \mathbf{N}_{\bar{k}_{\mathrm{rp}}} \mathbf{N}_{\bar{k}_{\mathrm{rp}}}^T \mathrm{d}\bar{k}_{\mathrm{rp}} + \\ E_{\mathrm{r}} I_{\mathrm{r}} \int_{I_{k_y}} k_y^4 \mathbf{N}_{k_y} \mathbf{N}_{k_y}^T \mathrm{d}k_y \otimes \int_{I_\omega} \mathbf{N}_\omega \mathbf{N}_\omega^T \mathrm{d}\omega \otimes \int_{I_{\bar{k}_{\mathrm{rp}}}} \mathbf{N}_{\bar{k}_{\mathrm{rp}}} \mathbf{N}_{\bar{k}_{\mathrm{rp}}}^T \mathrm{d}\bar{k}_{\mathrm{rp}}\end{aligned} \tag{14}$$

Note that the stiffness operator $\mathcal{A}$ allows efficient multiplication with the displacements and test functions due to its Kronecker form:

$$\mathcal{A} = \sum_{r_A=1}^{R_A} A_{k_y}^{r_A} \otimes A_{\omega}^{r_A} \otimes A_{\bar{k}_{\mathrm{rp}}}^{r_A} \tag{15}$$

The resulting system of equations is non-linear as the displacement tensor $\mathcal{U}$ contains a product of the unknown nodal values $\underline{\mathbf{u}}_k^{R_u+1}$. As all displacement vectors at previous iterations (1 until R_u) are known, six variables remain unknown, consisting of three displacement vectors ($\underline{\mathbf{u}}_{k_y}^{R_u+1}$, $\underline{\mathbf{u}}_{\omega}^{R_u+1}$ and $\underline{\mathbf{u}}_{\bar{k}_{\mathrm{rp}}}^{R_u+1}$) and three test functions ($\underline{\mathbf{v}}_{k_y}$, $\underline{\mathbf{v}}_{\omega}$ and $\underline{\mathbf{v}}_{\bar{k}_{\mathrm{rp}}}$).

To solve the system of equations, the test functions have to be further specified. Use can be made of either a Galerkin or Petrov-Galerkin strategy. The first option is used in the standard PGD methodology and represents an orthogonal projection of the residual as the set of test functions equals the set of displacements

($\mathcal{V} = \mathcal{U}$). In the Petrov-Galerkin strategy, an oblique projection is performed and additional equations have to be specified to determine the test functions. This alternative approach is discussed in section 2.3.

Implementation of the Galerkin conditions ($\underline{\mathbf{v}}_{k_y} = \underline{\mathbf{u}}_{k_y}^{R_u+1}$,$\underline{\mathbf{v}}_{\omega} = \underline{\mathbf{u}}_{\omega}^{R_u+1}$ and $\underline{\mathbf{v}}_{\bar{k}_{\mathrm{rp}}} = \underline{\mathbf{u}}_{\bar{k}_{\mathrm{rp}}}^{R_u+1}$) reduces the number of unknowns to three. The non-linear problem in equation (9) is solved using an alternating direction strategy [5].

First, the equations are solved for the unknown displacement vector $\underline{\mathbf{u}}_{k_y}^{R_u+1}$. The other unknowns are initialized using random unitary vectors. The equilibrium equations then reduce to:

$$\begin{aligned}
&\text{Find } \underline{\mathbf{u}}_{k_y}^{R_u+1} \in \mathbb{C}^{N_{k_y}} \text{ such that :} \\
&\left(\underline{\mathbf{v}}_{k_y} \otimes \underline{\mathbf{u}}_{\omega}^{R_u+1} \otimes \underline{\mathbf{u}}_{\bar{k}_{\mathrm{rp}}}^{R_u+1}\right)^{\mathbf{H}} \mathcal{A} \left(\underline{\mathbf{u}}_{k_y}^{R_u+1} \otimes \underline{\mathbf{u}}_{\omega}^{R_u+1} \otimes \underline{\mathbf{u}}_{\bar{k}_{\mathrm{rp}}}^{R_u+1}\right) = \\
&\left(\underline{\mathbf{v}}_{k_y} \otimes \underline{\mathbf{u}}_{\omega}^{R_u+1} \otimes \underline{\mathbf{u}}_{\bar{k}_{\mathrm{rp}}}^{R_u+1}\right)^{\mathbf{H}} \mathcal{F} - \left(\underline{\mathbf{v}}_{k_y} \otimes \underline{\mathbf{u}}_{\omega}^{R_u+1} \otimes \underline{\mathbf{u}}_{\bar{k}_{\mathrm{rp}}}^{R_u+1}\right)^{\mathbf{H}} \mathcal{A}\mathcal{U}_0 \qquad \forall \underline{\mathbf{v}}_{k_y} \in \mathbb{C}^{N_{k_y}}
\end{aligned} \tag{16}$$

This can be further elaborated when taking into account that $\underline{\mathbf{v}}_{k_y}$ is arbitrary:

$$\begin{aligned}
&\text{Find } \underline{\mathbf{u}}_{k_y}^{R_u+1} \in \mathbb{C}^{N_{k_y}} \text{ such that :} \\
&\left(\mathbf{I}_{k_y} \otimes \underline{\mathbf{u}}_{\omega}^{R_u+1} \otimes \underline{\mathbf{u}}_{\bar{k}_{\mathrm{rp}}}^{R_u+1}\right)^{\mathbf{H}} \mathcal{A} \left(\underline{\mathbf{u}}_{k_y}^{R_u+1} \otimes \underline{\mathbf{u}}_{\omega}^{R_u+1} \otimes \underline{\mathbf{u}}_{\bar{k}_{\mathrm{rp}}}^{R_u+1}\right) = \\
&\left(\mathbf{I}_{k_y} \otimes \underline{\mathbf{u}}_{\omega}^{R_u+1} \otimes \underline{\mathbf{u}}_{\bar{k}_{\mathrm{rp}}}^{R_u+1}\right)^{\mathbf{H}} \mathcal{F} - \left(\mathbf{I}_{k_y} \otimes \underline{\mathbf{u}}_{\omega}^{R_u+1} \otimes \underline{\mathbf{u}}_{\bar{k}_{\mathrm{rp}}}^{R_u+1}\right)^{\mathbf{H}} \mathcal{A}\mathcal{U}_0
\end{aligned} \tag{17}$$

where $\mathbf{I}_{k_y}$ is an identity matrix of size N_{k_y}. This one-dimensional equation can be solved for the unknown displacement vector $\underline{\mathbf{u}}_{k_y}^{R_u+1}$. In a next step the displacement vector $\underline{\mathbf{u}}_{\omega}^{R_u+1}$ is updated by fixing $\underline{\mathbf{u}}_{k_y}^{R_u+1}$ and $\underline{\mathbf{u}}_{\bar{k}_{\mathrm{rp}}}^{R_u+1}$. Additionally, the vector is normalized. Finally, the displacement vector $\underline{\mathbf{u}}_{\bar{k}_{\mathrm{rp}}}^{R_u+1}$ is updated by fixing the remaining variables and the resulting vector is normalized. The normalization of all vectors except one ensures that the resulting rank-one tensor is uniquely defined. Alternatively, all vectors can be normalized and the rank-one contribution is given by:

$$\mathcal{U} = u_z^{R_u+1} \left(\underline{\mathbf{u}}_{k_y}^{R_u+1} \otimes \underline{\mathbf{u}}_{\omega}^{R_u+1} \otimes \underline{\mathbf{u}}_{\bar{k}_{\mathrm{rp}}}^{R_u+1}\right) \tag{18}$$

where $u_z^{R_u+1}$ is a scalar. Both methodologies are equivalent. The updating process is repeated until convergence, or until a maximum number of iterations is reached. The convergence criterion is specified in section 3.

The displacement vector is updated:

$$\mathcal{U}_0 = \sum_{r_u=1}^{R_u+1} \underline{\mathbf{u}}_{k_y}^{r_u} \otimes \underline{\mathbf{u}}_{\omega}^{r_u} \otimes \underline{\mathbf{u}}_{\bar{k}_{\mathrm{rp}}}^{r_u} \tag{19}$$

Convergence is then checked as elaborated in section 3. If the criterion is not fulfilled, a new rank-one contribution (enrichment $R_u + 2$) is computed using the updated value for $\mathcal{U}_0$.

2.2 PGD for a 2.5D ballast track

The dynamic response of a ballast track is considered. It is assumed that the material properties and geometry of the track, embankment and soil do not vary in the longitudinal direction $\mathbf{e}_y$ parallel to the track, so that the coordinate y can be transformed to the wavenumber k_y and the problem can be formulated in the wavenumber-frequency domain. A two-and-a-half dimensional (2.5D) finite element (FE) model is used, as illustrated in figure 1b, significantly reducing the computational effort. As a result, the finite element

discretization is only introduced in the cross section and the displacement vector $\hat{\mathbf{u}}(x, y, z, \omega)$ is discretized as:

$$\hat{\mathbf{u}}(x, y, z, \omega) \simeq \mathbf{N}_{xz}(x, z)\underline{\hat{\mathbf{u}}}(y, \omega) \tag{20}$$

where a hat above a variable denotes its representation in the frequency domain, $\mathbf{N}(x, z)$ holds the shape functions in the cross section and $\underline{\hat{\mathbf{u}}}(y, \omega)$ is the displacement vector along all degrees of freedom of the 2D mesh.

Semi-analytical models are used for the track components. The rails are modelled as Euler-Bernoulli beams with cross section A_r, moment of inertia I_r, Young's modulus E_r and density ρ_r. Their kinematics is restricted to a vertical displacement. The rail pads have a stiffness k_rp and loss factor η_rp. This stiffness is distributed in the longitudinal direction as $\bar{k}_\mathrm{rp} = k_\mathrm{rp}/d$, with d the sleeper distance. The sleepers have a mass m_sl and rotational inertia I_sl that are smeared in the longitudinal direction as $\bar{m}_\mathrm{sl} = m_\mathrm{sl}/d$ and $\bar{I}_\mathrm{sl} = I_\mathrm{sl}/d$. Rigid body kinematics are assumed for the sleepers in terms of their vertical displacement and rotation. Therefore, the movement of the interface between the sleeper and ballast is restricted to rigid body kinematics by means of constraint equations. The sleepers do not contribute to the longitudinal stiffness of the track.

The ballast directly next to and in between the sleepers is added as extra mass. The remaining ballast is modelled by means of a 2.5D finite element formulation assuming linear elastic isotropic soil behaviour. This is described by means of five material properties: the shear wave velocity C_s, the dilatational wave velocity C_p, the density ρ and the hysteretic material damping ratio in shear and dilatational deformation β_s and β_p. Relative motion and friction between grains in the solid skeleton or presence of moisture in the pores results in energy dissipation or material damping. This can be accounted for in the frequency domain by means of the correspondence principle where both Lamé coefficients are replaced by the following complex moduli:

$$\mu^* = \mu(1 + 2\beta_\mathrm{s}\mathrm{i}); \qquad (\lambda + 2\mu)^* = (\lambda + 2\mu)(1 + 2\beta_\mathrm{p}\mathrm{i}) \tag{21}$$

These complex Lamé coefficients in turn result in complex wave velocities C_s^* and C_p^*. The 2.5D finite element equations are derived following a standard Galerkin procedure where the test functions $\hat{\mathbf{v}}(x, y, z, \omega)$ use the same discretization as the displacement vector $\hat{\mathbf{u}}(x, y, z, \omega)$:

$$\hat{\mathbf{v}}(x, y, z, \omega) \simeq \mathbf{N}_{xz}(x, z)\underline{\hat{\mathbf{v}}}(y, \omega) \tag{22}$$

The underlying halfspace is modelled by means of a Boundary Element Method (BEM) [13]. The displacements of the interface between the ballast and soil are restricted to in-plane rigid body kinematics consisting of a vertical translation and rotation around its centre. This restriction is achieved through constraint equations. The soil stiffness matrix $K_\mathrm{s}(p_y, \omega)$ depends on the frequency and slowness $p_y = k_y/\omega$, accounting for both rotational and translational stiffness as well as damping.

The coupling of the 2.5D semi-analytical and finite element equations for track and embankment, combined with the soil stiffness, results in the following system of equations [3, 13]:

$$\left[-\omega^2\mathbf{M} + \mathbf{K}_0 - \mathrm{i}p_y\omega\mathbf{K}_1 - p_y^2\omega^2\mathbf{K}_2 + p_y^4\omega^4\mathbf{K}_4 + \mathbf{K}_\mathrm{s}(p_y, \omega)\right]\underline{\tilde{\mathbf{u}}}(p_y, \omega) = \tilde{\mathbf{f}}(p_y, \omega) \tag{23}$$

where a tilde above a variable denotes its representation in the slowness-frequency domain.

The PGD methodology is used to solve equation (23). A weak form and discretization with respect to the in-plane coordinates has already been introduced as the finite element method was used in the cross-section with domain I_{xz}, resulting in displacement values in $\mathcal{K}_{xz}$. Additionally, a range of slowness values on I_{p_y} is considered, resulting in displacement values in $\mathcal{K}_{p_y}$, and frequencies in I_ω, with displacements in $\mathcal{K}_\omega$. The displacement vector can be approximated as:

$$\tilde{\mathbf{u}}(x, p_y, z, \omega) \simeq \sum_{r_u=1}^{R_u} \mathbf{u}_{xz}^{r_u}(x, z)\mathbf{u}_{p_y}^{r_u}(p_y)\mathbf{u}_\omega^{r_u}(\omega) \tag{24}$$

All domains are discretized using N_{xz}, N_{p_y} and N_ω samples for the in-plane coordinate, slowness and

frequency, respectively. The number of samples in the spatial domain coincides with the total number of degrees of freedom. The shape functions are grouped in the matrices $\mathbf{N}_{xz}$, $\mathbf{N}_{p_y}$ and $\mathbf{N}_{\omega}$, resulting in:

$$\tilde{\mathbf{u}}(x,p_y,z,\omega) \simeq \sum_{r_u=1}^{R_u+1} \left(\mathbf{N}_{xz}\underline{\mathbf{u}}_{xz}^{r_u}\right)\left(\mathbf{N}_{p_y}\underline{\mathbf{u}}_{p_y}^{r_u}\right)\left(\mathbf{N}_{\omega}\underline{\mathbf{u}}_{\omega}^{r_u}\right) \tag{25}$$

Making use of equation (20), this is equivalent to:

$$\underline{\tilde{\mathbf{u}}}(p_y,\omega) \simeq \sum_{r_u=1}^{R_u+1} \underline{\mathbf{u}}_{xz}^{r_u}\left(\mathbf{N}_{p_y}\underline{\mathbf{u}}_{p_y}^{r_u}\right)\left(\mathbf{N}_{\omega}\underline{\mathbf{u}}_{\omega}^{r_u}\right) \tag{26}$$

The same discretization is used for the test functions:

$$\tilde{\mathbf{v}}(x,p_y,z,\omega) \simeq \left(\mathbf{N}_{xz}\underline{\mathbf{v}}_{xz}\right)\left(\mathbf{N}_{p_y}\underline{\mathbf{v}}_{p_y}\right)\left(\mathbf{N}_{\omega}\underline{\mathbf{v}}_{\omega}\right) \tag{27}$$

Making use of equation (22), this can be rewritten as:

$$\underline{\tilde{\mathbf{v}}}(p_y,\omega) \simeq \underline{\mathbf{v}}_{xz}\left(\mathbf{N}_{p_y}\underline{\mathbf{v}}_{p_y}\right)\left(\mathbf{N}_{\omega}\underline{\mathbf{v}}_{\omega}\right) \tag{28}$$

The weighted residual formulation can be deduced from equation (23):

$$\begin{aligned}
&\text{Find } \underline{\mathbf{u}}_{xz}^{R_u+1} \in \mathbb{C}^{N_{xz}},\ \underline{\mathbf{u}}_{p_y}^{R_u+1} \in \mathbb{C}^{N_{p_y}} \text{ and } \underline{\mathbf{u}}_{\omega}^{R_u+1} \in \mathbb{C}^{N_{\omega}} \text{ such that :}\\
&\int_{I_{p_y}\times I_{\omega}} \left[\underline{\mathbf{v}}_{xz}\otimes\left(\mathbf{N}_{p_y}\underline{\mathbf{v}}_{p_y}\right)\otimes\left(\mathbf{N}_{\omega}\underline{\mathbf{v}}_{\omega}\right)\right]^{\mathbf{H}}\left[-\omega^2\mathbf{M}+\mathbf{K}_0-\mathrm{i}p_y\omega\mathbf{K}_1-p_y^2\omega^2\mathbf{K}_2+p_y^4\omega^4\mathbf{K}_4+\mathbf{K}_{\mathrm{s}}(p_y,\omega)\right]\\
&\qquad\left[\sum_{r_u=1}^{R_u+1}\left[\underline{\mathbf{u}}_{xz}^{r_u}\otimes\left(\mathbf{N}_{p_y}\underline{\mathbf{u}}_{p_y}^{r_u}\right)\otimes\left(\mathbf{N}_{\omega}\underline{\mathbf{u}}_{\omega}^{r_u}\right)\right]\right]\,\mathrm{d}p_y\mathrm{d}\omega\\
&\qquad=\int_{I_{p_y}\times I_{\omega}}\left[\underline{\mathbf{v}}_{xz}\otimes\left(\mathbf{N}_{p_y}\underline{\mathbf{v}}_{p_y}\right)\otimes\left(\mathbf{N}_{\omega}\underline{\mathbf{v}}_{\omega}\right)\right]^{\mathbf{H}}\tilde{\mathbf{f}}(p_y,\omega)\,\mathrm{d}p_y\mathrm{d}\omega\\
&\qquad\qquad\forall\,\underline{\mathbf{v}}_{xz}\in\mathbb{C}^{N_{xz}},\ \underline{\mathbf{v}}_{p_y}\in\mathbb{C}^{N_{p_y}},\ \underline{\mathbf{v}}_{\omega}\in\mathbb{C}^{N_{\omega}}
\end{aligned} \tag{29}$$

Use of the alternating direction scheme discussed in section 2.1 is only feasible when the stiffness matrix has a Kronecker form. This is hindered by the structure of the soil stiffness matrix $\mathbf{K}_{\mathrm{s}}(p_y,\omega)$. An approximate separated form is computed by means of the Canonical Polyadic Decomposition (CPD) as a sum of rank-one tensors:

$$\mathbf{K}_{\mathrm{s}}(p_y,\omega) \simeq \sum_{r_K=1}^{R_K}\mathbf{K}_{xz}\otimes\mathbf{k}_{p_y}^{r_K}\otimes\mathbf{k}_{\omega}^{r_K} \tag{30}$$

where the matrix $\mathbf{K}_{xz}$ is equal to one for the degrees of freedom coinciding with the translational and rotational displacement of the interface and zero otherwise. The rank R_K of the decomposition should consider both the accuracy of the solution and the computation time. The applied force also has a separated representation:

$$\tilde{\mathbf{f}}(p_y,\omega) = \sum_{r_f=1}^{R_f}\mathbf{f}_{xz}\otimes\mathbf{f}_{p_y}^{r_f}\otimes\mathbf{f}_{\omega}^{r_f} \tag{31}$$

where the vector $\mathbf{f}_{xz}$ gives the spatial variation of the load. After including the separated forms, the system of equations can be rewritten as:

$$\begin{aligned}
&\text{Find } \underline{\mathbf{u}}_{xz}^{R_u+1} \in \mathbb{C}^{N_{xz}},\ \underline{\mathbf{u}}_{p_y}^{R_u+1} \in \mathbb{C}^{N_{p_y}} \text{ and } \underline{\mathbf{u}}_{\omega}^{R_u+1} \in \mathbb{C}^{N_{\omega}} \text{ such that :}\\
&\qquad\mathcal{V}^{\mathbf{H}}\mathcal{A}\mathcal{U}=\mathcal{V}^{\mathbf{H}}\mathcal{F}-\mathcal{V}^{\mathbf{H}}\mathcal{A}\mathcal{U}_0\qquad\forall\,\underline{\mathbf{v}}_{xz}\in\mathbb{C}^{N_{xz}},\underline{\mathbf{v}}_{p_y}\in\mathbb{C}^{N_{p_y}},\underline{\mathbf{v}}_{\omega}\in\mathbb{C}^{N_{\omega}}
\end{aligned} \tag{32}$$

with $\mathcal{U}_0$ a tensor containing all nodal values computed in previous enrichments:

$$\mathcal{U}_0 = \sum_{r_u=1}^{R_u} \underline{\mathbf{u}}_{xz}^{r_u} \otimes \underline{\mathbf{u}}_{p_y}^{r_u} \otimes \underline{\mathbf{u}}_{\omega}^{r_u} \tag{33}$$

$\mathcal{U}$ a tensor containing all unknown nodal values:

$$\mathcal{U} = \underline{\mathbf{u}}_{xz}^{R_u+1} \otimes \underline{\mathbf{u}}_{p_y}^{R_u+1} \otimes \underline{\mathbf{u}}_{\omega}^{R_u+1} \tag{34}$$

$\mathcal{V}$ a tensor with the nodal values of the test functions:

$$\mathcal{V} = \underline{\mathbf{v}}_{xz} \otimes \underline{\mathbf{v}}_{p_y} \otimes \underline{\mathbf{v}}_{\omega} \tag{35}$$

$\mathcal{F}$ the force operator:

$$\mathcal{F} = \sum_{r_f=1}^{R_f} \mathbf{f}_{xz} \otimes \int_{I_{p_y}} \mathbf{N}_{p_y} \mathbf{f}_{p_y}^{r_f} \mathrm{d}p_y \otimes \int_{I_\omega} \mathbf{N}_\omega \mathbf{f}_\omega^{r_f} \mathrm{d}\omega \tag{36}$$

and $\mathcal{A}$ the stiffness operator:

$$\begin{aligned}\mathcal{A} = \mathbf{M} \otimes \int_{I_{p_y}} \mathbf{N}_{p_y}\mathbf{N}_{p_y}^T \mathrm{d}p_y \otimes \int_{I_\omega} -\omega^2 \mathbf{N}_\omega \mathbf{N}_\omega^T \mathrm{d}\omega + \mathbf{K}_0 \otimes \int_{I_{p_y}} \mathbf{N}_{p_y}\mathbf{N}_{p_y}^T \mathrm{d}p_y \otimes \int_{I_\omega} \mathbf{N}_\omega \mathbf{N}_\omega^T \mathrm{d}\omega + \\ \mathbf{K}_1 \otimes \int_{I_{p_y}} -\mathrm{i}p_y \mathbf{N}_{p_y}\mathbf{N}_{p_y}^T \mathrm{d}p_y \otimes \int_{I_\omega} \omega \mathbf{N}_\omega \mathbf{N}_\omega^T \mathrm{d}\omega + \mathbf{K}_2 \otimes \int_{I_{p_y}} -p_y^2 \mathbf{N}_{p_y}\mathbf{N}_{p_y}^T \mathrm{d}p_y \otimes \int_{I_\omega} \omega^2 \mathbf{N}_\omega \mathbf{N}_\omega^T \mathrm{d}\omega + \\ \mathbf{K}_4 \otimes \int_{I_{p_y}} p_y^4 \mathbf{N}_{p_y}\mathbf{N}_{p_y}^T \mathrm{d}p_y \otimes \int_{I_\omega} \omega^4 \mathbf{N}_\omega \mathbf{N}_\omega^T \mathrm{d}\omega + \mathbf{K}_{xz} \otimes \int_{I_{p_y}} k_{p_y}^1 \mathbf{N}_{p_y}\mathbf{N}_{p_y}^T \mathrm{d}p_y \otimes \int_{I_\omega} k_\omega^1 \mathbf{N}_\omega \mathbf{N}_\omega^T \mathrm{d}\omega + ... + \\ \mathbf{K}_{xz} \otimes \int_{I_{p_y}} k_{p_y}^{R_k} \mathbf{N}_{p_y}\mathbf{N}_{p_y}^T \mathrm{d}p_y \otimes \int_{I_\omega} k_\omega^{R_k} \mathbf{N}_\omega \mathbf{N}_\omega^T \mathrm{d}\omega\end{aligned} \tag{37}$$

Equation (32) is equivalent to equation (9) derived for the beam on a Winkler foundation. The same solution strategy can therefore be adapted.

2.3 Alternative PGD formulations

In standard Galerkin PGD the energy norm of the error is minimized by means of an orthogonal projection on the approximation space. A first alternative formulation introduces a Petrov-Galerkin approach, where an oblique projection is performed. A second alternative uses a different norm in the minimization problem, resulting in a minimal residual approach. Both alternatives are briefly discussed and compared subsequently to the standard Galerkin PGD.

2.3.1 Petrov-Galerkin approach

For non-Hermitian problems, as presented in this paper, the use of an oblique projection can be favourable [8]. An additional system of equations is considered to determine each test function $\underline{\mathbf{v}}_k$ corresponding to variable k. As a result, N additional systems of equations are considered, consisting of an additional orthogonality criterion for each variable k [7]:

$$\begin{aligned}&\text{Find } \underline{\mathbf{v}}_k \in \mathbb{C}^{N_k} \text{ such that :} \\ &\mathcal{V}^H \mathcal{A} \left(\underline{\mathbf{u}}_1^{R_u+1} \otimes \cdots \otimes \underline{\mathbf{u}}_k^* \otimes \cdots \otimes \underline{\mathbf{u}}_N^{R_u+1} \right) = < \left(\underline{\mathbf{u}}_1^{R_u+1} \otimes \cdots \otimes \underline{\mathbf{u}}_k^* \otimes \cdots \otimes \underline{\mathbf{u}}_N^{R_u+1} \right), \mathcal{U} >_{\mathrm{N}} \\ &\qquad\qquad \forall \underline{\mathbf{u}}_k^* \in \mathbb{C}^{N_k}\end{aligned} \tag{38}$$

with $< \cdot >_N$ an inner product on the N-dimensional displacement space. In the examples, a classical inner product in L^2 is considered. The inner product is illustrated for the beam on a Winkler foundation for two displacement fields u_z and w_z:

$$\begin{aligned} < u_z, w_z >_3 &= < u_z, w_z >_{L^2(I_{k_y})\otimes L^2(I_\omega)\otimes L^2(I_{\bar{k}_{\mathrm{rp}}})} \\ &= \int_{I_{k_y}}\int_{I_\omega}\int_{I_{\bar{k}_{\mathrm{rp}}}} u_z(k_y,\omega,\bar{k}_{\mathrm{rp}}) w_z(k_y,\omega,\bar{k}_{\mathrm{rp}})\, \mathrm{d}k_y \mathrm{d}\omega \mathrm{d}\bar{k}_{\mathrm{rp}} \\ &\simeq \int_{I_{k_y}}\int_{I_\omega}\int_{I_{\bar{k}_{\mathrm{rp}}}} \left[\left(\mathbf{N}_{k_y}^{\mathrm{T}}\underline{\mathbf{u}}_{k_y}\right)\left(\mathbf{N}_{\omega}^{\mathrm{T}}\underline{\mathbf{u}}_{\omega}\right)\left(\mathbf{N}_{\bar{k}_{\mathrm{rp}}}^{\mathrm{T}}\underline{\mathbf{u}}_{\bar{k}_{\mathrm{rp}}}\right)\right]^H \\ &\quad \left[\left(\mathbf{N}_{k_y}^{\mathrm{T}}\underline{\mathbf{w}}_{k_y}\right)\left(\mathbf{N}_{\omega}^{\mathrm{T}}\underline{\mathbf{w}}_{\omega}\right)\left(\mathbf{N}_{\bar{k}_{\mathrm{rp}}}^{\mathrm{T}}\underline{\mathbf{w}}_{\bar{k}_{\mathrm{rp}}}\right)\right]\, \mathrm{d}k_y \mathrm{d}\omega \mathrm{d}\bar{k}_{\mathrm{rp}} \\ &= \left[\underline{\mathbf{u}}_{k_y}\int_{I_{k_y}} \mathbf{N}_{k_y}\mathbf{N}_{k_y}^{\mathrm{T}}\, \mathrm{d}k_y \underline{\mathbf{w}}_{k_y}\right] \otimes \left[\underline{\mathbf{u}}_{\omega}\int_{I_\omega} \mathbf{N}_{\omega}\mathbf{N}_{\omega}^{\mathrm{T}}\, \mathrm{d}\omega \underline{\mathbf{w}}_{\omega}\right] \otimes \left[\underline{\mathbf{u}}_{\bar{k}_{\mathrm{rp}}}\int_{I_{\bar{k}_{\mathrm{rp}}}} \mathbf{N}_{\bar{k}_{\mathrm{rp}}}\mathbf{N}_{\bar{k}_{\mathrm{rp}}}^{\mathrm{T}}\, \mathrm{d}\bar{k}_{\mathrm{rp}} \underline{\mathbf{w}}_{\bar{k}_{\mathrm{rp}}}\right] \end{aligned} \tag{39}$$

The integrals only have to be evaluated once. The additional orthogonality equations are considered in the alternating direction scheme as follows: 1) the displacement vector $\underline{\mathbf{u}}_k^{R_u+1}$ is computed by fixing the remaining variables, 2) the updated displacement vector $\underline{\mathbf{u}}_k^{R_u+1}$ is used in equation (38) to evaluate the corresponding test function $\mathbf{v}_k$. Consequently, the number of linear systems to evaluate in each iteration of the alternating direction scheme is doubled.

2.3.2 Minimal residual approach

In the minimal residual approach, the residual is minimized in each enrichment. This corresponds to solving [14, 12]:

$$\mathcal{U} \in \arg\min_{\mathcal{U}\in\mathcal{S}} \Pi(\mathcal{U}) = \frac{1}{2}\|\mathcal{A}(\mathcal{U}_0+\mathcal{U}) - \mathcal{F}\|_I^2 \tag{40}$$

with $\mathcal{S}$ the space of rank-one tensors and I the identity matrix. The objective function $\Pi(\mathcal{U})$ is elaborated as:

$$\Pi(\mathcal{U}) = \frac{1}{2}\mathcal{U}^H\mathcal{A}^H\mathcal{A}(\mathcal{U}_0+\mathcal{U}) - \mathcal{U}^H\mathcal{A}^H\mathcal{F} + \frac{1}{2}\mathcal{F}^H\mathcal{F} \tag{41}$$

The same solution strategy as for the standard PGD can be used when the stiffness operator $\mathcal{A}$ is substituted by $\mathcal{A}^H\mathcal{A}$ and the force operator $\mathcal{F}$ by $\mathcal{A}^H\mathcal{F}$. As a result, the number of factors in the Kronecker forms of both the stiffness and load operator strongly increases to R_A^2 and $R_A \cdot R_f$, respectively. Moreover, the condition number of the stiffness operator is squared, often leading to bad convergence rates [7].

3 Results

First, a beam on a Winkler foundation is used to illustrate the convergence behaviour of the PGD enrichments. Next, the 2.5D ballast track is considered for a track supported by both a homogeneous and layered halfspace.

The approximation spaces for the spatial variables are constructed using classic finite elements with three-node triangular elements. For the remaining variables, the approximation space is one-dimensional and third order local shape functions are used.

Within the fixed point iteration scheme, convergence is checked using solutions at subsequent iterations for each variable as:

$$\left\|\underline{\mathbf{u}}_k^{R_u+1,i} - \underline{\mathbf{u}}_k^{R_u+1,i-1}\right\|_2 < \epsilon \tag{42}$$

where k corresponds to the variable and i counts the number of fixed point iterations. This number is also limited to 100 to ensure that the fixed point iterations break down within reasonable time.

All results are computed considering the direct solution of the system of equations for all parameter combinations, as well as using the PGD algorithms. The error can be estimated as:

$$\epsilon_{R_u} = \frac{||\mathcal{U}_{R_u} - \mathcal{U}_{\text{an}}||_F}{||\mathcal{U}_{\text{an}}||_F} \tag{43}$$

with $\mathcal{U}_{R_u}$ the full displacement tensor computed with R_u PGD enrichments and $\mathcal{U}_{\text{an}}$ the direct solution of the equilibrium equations. $||\cdot||_F$ is the Frobenius norm of the tensor.

As the full solution is generally not available, alternative convergence criteria can be checked. The relative contribution of the current enrichment $\mathcal{U}$ to the total displacement tensor $\mathcal{U}_0$ can give an indication of convergence:

$$\frac{||\mathcal{U}||_F}{||\mathcal{U}_0||_F} < \epsilon \tag{44}$$

Alternatively, convergence can be checked based on the norm of the first enrichment $\mathcal{U}_1$, as this is generally cheaper to evaluate:

$$\frac{||\mathcal{U}||_F}{||\mathcal{U}_1||_F} < \epsilon \tag{45}$$

The validity of this criterion is discussed in the presented examples.

As discussed in section 2.3, the formulation of the PGD can be altered as well as the projection. Four different algorithms can be distinguished:

- PGD-G: minimization of the energy norm of the error using an orthogonal projection;
- PGD-PG: minimization of the energy norm of the error using an oblique projection;
- MinRes-G: minimization of the 2-norm of the residual using an orthogonal projection;
- MinRes-PG: minimization of the 2-norm of the residual using an oblique projection.

3.1 Beam on a Winkler foundation

The results are computed for a UIC60 rail with a mass per unit length $\rho_{\text{r}} A_{\text{r}}$ of 60.21 kg/m and bending stiffness $E_{\text{r}} I_{\text{r}}$ of 6.68 MNm^2. The rail pads have a variable stiffness with a nominal value of 255.7 MN/m^2. Damping is accounted for by means of a loss factor η_{rp} equal to 0.1. A vertical unit load is considered in the frequency-wavenumber domain to compute the transfer function of the rail.

The solution of equation (2) is used as a reference solution, from which the dispersion curve of the bending wave can be derived (for the case of zero damping):

$$k_y = \sqrt[4]{\frac{\rho_{\text{r}} A_{\text{r}} \omega^2 - \bar{k}_{\text{rp}}}{E_{\text{r}} I_{\text{r}}}} \tag{46}$$

The bending wave propagates through the rail starting from the cut-on frequency ω_{co}:

$$\omega_{\text{co}} = \sqrt{\frac{\bar{k}_{\text{rp}}}{\rho_{\text{r}} A_{\text{r}}}} \tag{47}$$

The cut-on frequency of the rail is included in the sampling for the full range of rail pad stiffness values. An overview of the sampling is given in table 1. All samples are linearly spaced.

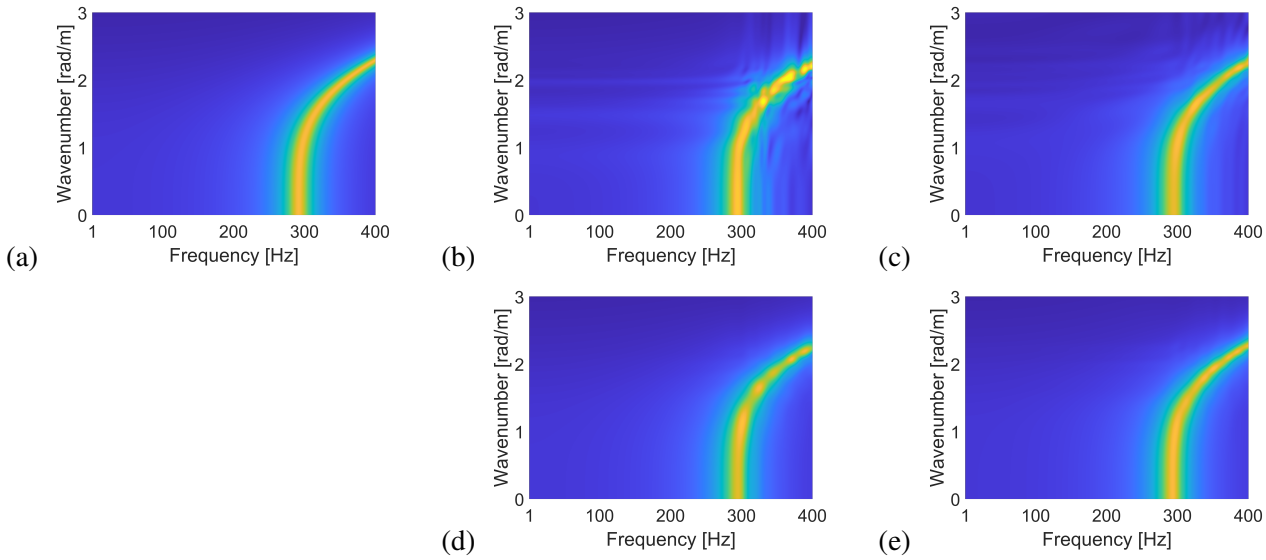

Figure 2: Modulus of the rail receptance as a function of frequency and wavenumber for a beam on a Winkler foundation with the lowest spring stiffness (204.6 $\mathrm{MN/m^2}$) using (a) the direct solution of the equilibrium equation, (b) PGD-G, (c) PGD-PG, (d) MinRes-G, and (e) MinRes-PG algorithm with 50 enrichments.

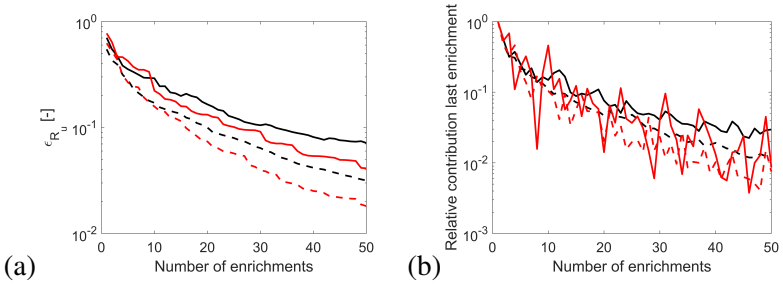

Figure 3: (a) Dimensionless error ϵ_{R_u}, and (b) relative contribution of last enrichment for the beam on a Winkler foundation for PGD-G (black solid line), PGD-PG (black dashed line), MinRes-G (red solid line), and MinRes-PG (red dashed line) approach.

Table 1: Sampling variables for the beam on a Winkler foundation.

Variable	Range	Number of samples
Frequency	1-400 Hz	400
Wavenumber	0-3 rad/m	400
Spring stiffness	$[0.8, 1.2] \cdot 255.7$ MN/m^2	61

The results are presented in the frequency-wavenumber domain for the lowest spring stiffness. The analytical solution is compared to the four methodologies in figure 2. The dimensionless error and convergence criterion are shown in figure 3. One can distinguish the bending wave as the zone of maximum response. Complex dynamic behaviour is found and more enrichments are needed to capture the displacements as is clear from figure 2b. The use of a Petrov-Galerkin approach results in quicker and smoother convergence for both the standard PGD and minimal residual approach, with overall faster convergence for the latter. However, the dimensionless error is still well above 0.01 after 50 enrichments for all algorithms. This indicates that, although some improvements are made, a high number of enrichments is still needed. The convergence criterion based on the relative contribution of the last enrichment proves to be quite stable for the standard PGD methodology, but strongly varies for the minimal residual formulation.

3.2 2.5D ballast track

The geometry is illustrated in figure 1b. The results are computed for a UIC60 rail as described in section 1b. The rail pads are of medium stiffness with a rail pad stiffness of 120 $\mathrm{MN/m^2}$ and loss factor of 0.15. The sleepers have a spacing of 0.67 m and each sleeper has dimensions 2.5 $\mathrm{m}\times$ 0.263 $\mathrm{m}\times$ 0.185 m. The ballast has a Young's modulus of 100 MPa, a Poisson's ratio of 0.35 and a density of 2000 $\mathrm{kg/m^3}$. The ballast has a lower width of 3.90 m, upper width of 3.30 m and height of 0.50 m.

For the underlying soil, two different cases are discussed: a homogeneous halfspace and a layer on a halfspace. The properties of the halfspace and layer are given in table 2.

Table 2: Soil parameters for the halfspace and layer.

	h [m]	C_s [m/s]	C_p [m/s]	ρ [$\mathrm{kg/m^3}$]	β_s [-]	β_p [-]
Layer	3	150	300	1800	0.025	0.025
Halfspace	∞	300	600	1800	0.025	0.025

The resulting soil stiffness matrices have to be separated using a CPD. As the halfspace shows non-dispersive behaviour, the displacements become less complex and only five CPD terms have to be considered. For the layered soil the number of CPD terms is increased to ten, resulting in a dimensionless error of 0.2%.

A 2D mesh is generated consisting of 744 degrees of freedom. For the other variables equidistant sampling is used as described in table 3. The slowness sampling results in dimensionless wavenumber values ranging from 0 until 3, where the dimensionless wavenumber is defined as $\bar{k}_y = k_y C_\mathrm{s}/\omega$, with C_s the lowest shear wave velocity.

Table 3: Sampling variables for the 2.5D ballast track.

Variable	Range	Number of samples
Frequency	1-49 Hz	49
Slowness	[0-3]/C_s s/m	151

The transfer function of the ballast track is computed in the slowness-frequency domain. The load is evenly distributed over both rails. Results are shown in the dimensionless wavenumber-frequency domain for the rail receptance. The reference solution consists of the direction solution of the equilibrium equations in equation (23), as shown in figure 4a for the homogeneous halfspace. The zone of maximum response corresponds to the non-dispersive Rayleigh wave in the underlying halfspace.

All methodologies are compared in figure 4. The dimensionless error is given in figure 5. The standard methodology allows to capture the rail displacements using only 10 enrichments. Both the Galerkin and Petrov-Galerkin methodology perform well, with slightly lower errors when using Petrov-Galerkin. The minimal residual methodology does not converge and negligible gain in accuracy is made when adding enrichments, either when using orthogonal or oblique projections. This can be caused by the increased ill-conditioning due to the substitution of $\mathcal{A}$ by $\mathcal{A}^H\mathcal{A}$. Moreover, computation times strongly increase due to the increased number of terms in the Kronecker form. The convergence criterion based on the relative contribution of the last enrichment strongly varies with the number of enrichments. The most stable result is found for the PGD-PG algorithm, although not completely monotonic. The values for the minimal residual strategies decrease with the number of enrichments although the solution does not converge, indicating that the criterion does not properly identify convergence.

The same comparison is made for the 2.5D ballast track supported by a layer on a halfspace. Only the results for the standard PGD methodology are depicted as the computation time for the minimal resiudal methodology is prohibiting. Moreover, the methodology is not guaranteed to converge as was noted for

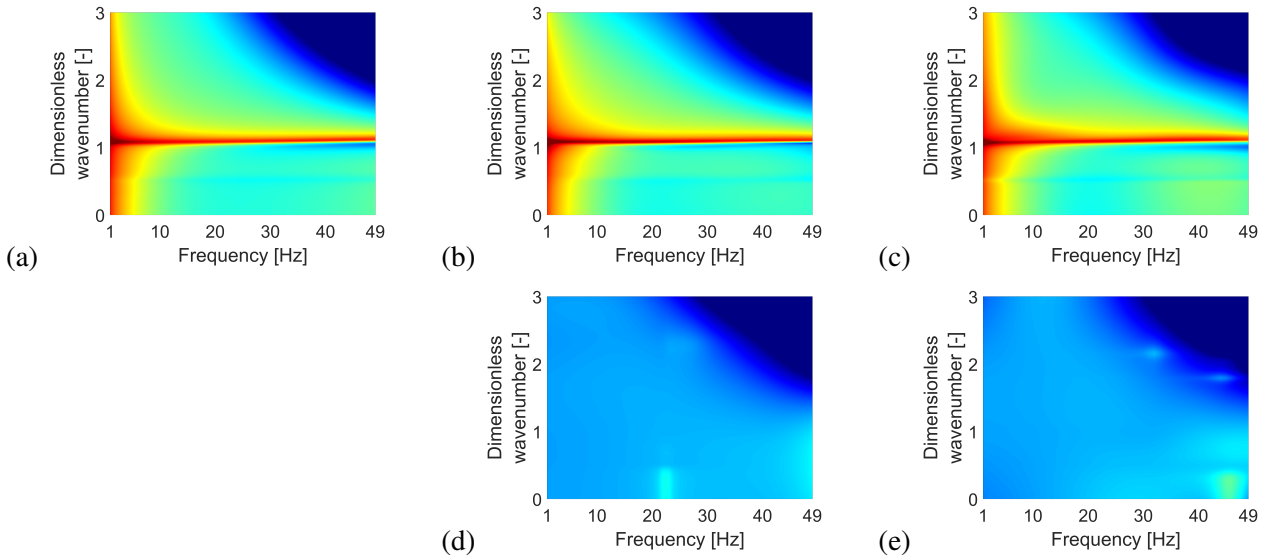

Figure 4: Logarithm of the modulus of the rail receptance for the ballast track on a homogeneous halfspace as a function of frequency and dimensionless wavenumber using (a) the direct solution of the equilibrium equations, the (b) PGD-G, (c) PGD-PG, (d) MinRes-G, and (e) MinRes-PG algorithm with 10 enrichments.

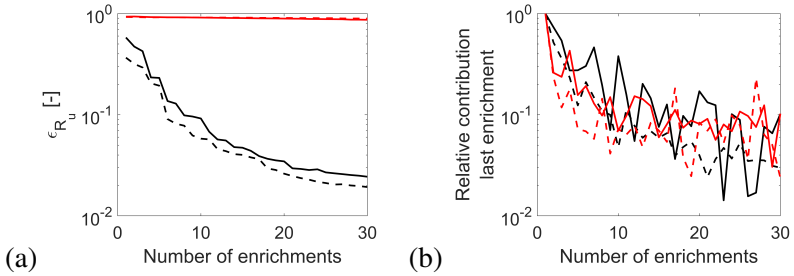

Figure 5: (a) Dimensionless error ϵ_{R_u}, and (b) relative contribution of the last enrichment for the ballast track on a homogeneous halfspace for PGD-G (black solid line), PGD-PG (black dashed line), MinRes-G (red solid line), and MinRes-PG (red dashed line) approach.

the ballast track on a homogeneous halfspace. Results for the rail receptance are depicted in figure 6 using 30 enrichments. This number is increased compared to the ballast track on a homogeneous halfspace as the displacement pattern becomes more intricate due to the dispersive behaviour of the underlying soil. The soil has multiple dispersion curves with different cut-on frequencies, corresponding to the zones of maximum response in figure 6a. Frequency-wavenumber combinations showing high displacements are well captured by both methodologies, however, the displacements in zones with low values seem disturbed. The dimensionless error, given in figure 7, stagnates at around 0.13, after which additional enrichments only provide small improvements. For the Petrov-Galerkin approach an increase in error is even observed. The convergence criterion based on the relative contribution of the last enrichment is again most stable for the PGD-PG algorithm. For the PGD-G algorithm, convergence can not be predicted based on the suggested criterion due to the large variations.

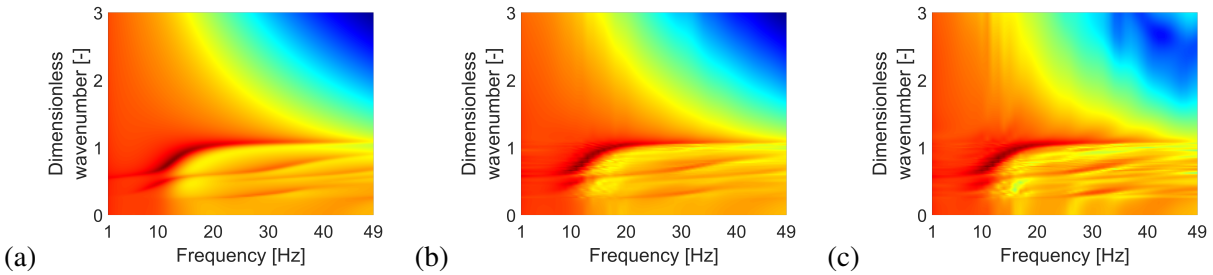

Figure 6: Logarithm of the modulus of the rail receptance for the ballast track on a layer on a halfspace as a function of frequency and dimensionless wavenumber using (a) the direct solution of the equilibrium equations, (b) the PGD-G, and (c) the PGD-PG algorithm with 30 enrichments.

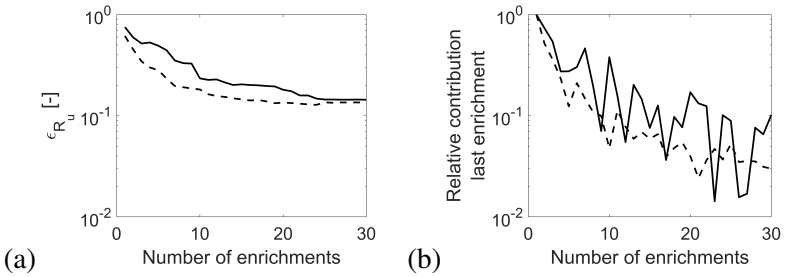

Figure 7: (a) Dimensionless error ϵ_{R_u}, and (b) relative contribution of the last enrichment for the ballast track on a layer on a halfspace for PGD-G (black solid line), and PGD-PG (black dashed line) approach.

4 Conclusion

This paper discusses the use of the Proper Generalized Decomposition for the prediction of railway induced vibrations in 2.5D track models. This a priori model order reduction technique computes a separated representation of the displacement field and permits the inclusion of additional parameters.

Four distinct PGD algorithms are defined and their use is first illustrated for a beam on a Winkler foundation. All algorithms converge and the benefit of the Petrov-Galerkin over the Galerkin approach is clear, both when using a standard PGD and minimal residual approach.

Results for a 2.5D ballast track are computed for both a homogeneous halfspace and a layer on a halfspace. The non-separability of the soil stiffness, computed using a BEM, is circumvented by the use of a CPD. The computation of a separable soil stiffness could be feasible using a PGD strategy and is subject for future research. For the homogeneous halfspace the solution converges for the standard PGD and a satisfactory error is found within a reasonable number of enrichments, both when using orthogonal and oblique projections. The minimal residual algorithm does not converge and CPU time is strongly increased. For the layer on a halfspace, the soil becomes dispersive, resulting in the need for more enrichments. The dimensionless error stagnates at 0.13 indicating that the greedy PGD strategy no longer extracts new information.

Acknowledgements

The research presented in this paper was performed within the frame of the project C14/20/073 “Model order reduction techniques for the prediction of railway induced vibration in the built environment” funded by the Research Council of KU Leuven. The financial support is gratefully acknowledged.

References

[1] L. Andersen and S. Nielsen, "Boundary element analysis of the steady-state response of an elastic half-space to a moving force on its surface," *Engineering Analysis with Boundary Elements*, vol. 27, pp. 23–38, 2003.

[2] J. Park and A. Kaynia, "FE simulation of steady state wave motion in solids combined with a PML approach," *Procedia Engineering*, vol. 199, pp. 1556–1561, 2017.

[3] S. François, M. Schevenels, G. Lombaert, and G. Degrande, "A 2.5D displacement based PML for elastodynamic wave propagation," *International Journal for Numerical Methods in Engineering*, vol. 90, no. 7, pp. 819–837, 2012. [Online]. Available: http://dx.doi.org/10.1002/nme.3344

[4] P. Galvín, S. François, M. Schevenels, E. Bongini, G. Degrande, and G. Lombaert, "A 2.5D coupled FE-BE model for the prediction of railway induced vibrations," *Soil Dynamics and Earthquake Engineering*, vol. 30, no. 12, pp. 1500–1512, 2010. [Online]. Available: http://dx.doi.org/10.1016/j.soildyn.2010.07.001

[5] F. Chinesta, R. Keunings, and A. Leygue, *The proper generalized decomposition for advanced numerical simulations. A primer*, 2014.

[6] F. Chinesta, A. Leygue, F. Bordeu, J. V. Aguado, E. Cueto, D. González, I. Alfaro, A. Ammar, and A. Huerta, "PGD-based computational vademecum for efficient design, optimization and control," *Archives of Computational methods in Engineering*, vol. 20, no. 1, pp. 31–59, 2013.

[7] A. Nuoy, "A priori model reduction through Proper Generalized Decomposition for solving time-dependent partial differential equations," *Computer Methods in Applied Mechanics and Engineering*, vol. 199(23-24), pp. 1603–1626, 2010.

[8] M. David, S. Zlotnik, and A. Huerta, "Proper generalized decomposition for parametrized Helmholtz problems in heterogeneous and unbounded domains: Application to harbor agitation," *Computer Methods in Applied Mechanics and Engineering*, vol. 295, pp. 127–149, 2015.

[9] R. Othman, A. Ammar, and K. H. Almitani, "Reduced modelling computation of layered soil's harmonic green functions," *Finite Elements in Analysis and Design*, vol. 177, p. 103419, 2020. [Online]. Available: https://www.sciencedirect.com/science/article/pii/S0168874X20300998

[10] M. Chevreuil and A. Nouy, "Model Order Reduction based on Proper Generalized Decomposition for the Propagation of Uncertainties in Structural Dynamics," *International Journal for Numerical Methods in Engineering*, vol. 89, pp. 241–268, 2012. [Online]. Available: https://hal.archives-ouvertes.fr/hal-00603342

[11] M. H. Malik, D. Borzacchiello, J. V. Aguado, and F. Chinesta, "Advanced parametric space-frequency separated representations in structural dynamics: A harmonic–modal hybrid approach," *Comptes Rendus Mécanique*, vol. 346, no. 7, pp. 590–602, 2018. [Online]. Available: https://www.sciencedirect.com/science/article/pii/S1631072118300743

[12] F. Qu, "Proper Generalized Decomposition for structural dynamics problems," Master's thesis, Technical University of Munich and KU Leuven, 2019.

[13] S. François, M. Schevenels, G. Lombaert, P. Galvín, and G. Degrande, "A 2.5D coupled FE-BE methodology for the dynamic interaction between longitudinally invariant structures and a layered halfspace," *Computer Methods in Applied Mechanics and Engineering*, vol. 199, no. 23-24, pp. 1536–1548, 2010. [Online]. Available: http://dx.doi.org/10.1016/j.cma.2010.01.001

[14] M. Chevreuil and A. Nouy, "Model Order Reduction based on Proper Generalized Decomposition for the Propagation of Uncertainties in Structural Dynamics," *International Journal for Numerical Methods in Engineering*, vol. 89, pp. 241–268, 2012. [Online]. Available: https://hal.archives-ouvertes.fr/hal-00603342